Design of bypass-simulated moving bed chromatography for reduced purity requirements

Maruyama Rafael, Karnal Preetika, Sainio Tuomo, Rajendran Arvind

DOI: 10.1016/j.ces.2019.05.003

Bypass-SMB: Enhancing simulated moving bed performance for reduced purity requirements

Rafael Teruo Maruyama[a], Preetika Karnal[b], Tuomo Sainio[c], Arvind Rajendran[a,*]

[a]*Department of Chemical and Materials Engineering, University of Alberta, 12th Floor, Donadeo Innovation Centre for Engineering (ICE), 9211-116 Street, Edmonton, Alberta, Canada T6G 1H9*

[b]*Department of Chemical and Biomolecular Engineering, Johns Hopkins University, 3400 N Charles Street, Baltimore, MD 21210, USA*

[c]*LUT University, School of Engineering Science, Skinnarilankatu 34, FI-53850 Lappeenranta, Finland*

Abstract

Bypass-Simulated moving bed (BP-SMB) chromatography, a process characterized by the possibility of over-purifying either the raffinate or the extract product followed by blending with the feed, is studied. The BP-SMB provides additional degrees of freedom; the opportunity to increase productivity; increased robustness and operational flexibility compared to obtaining reduced purities directly from the SMB. Based on the local-equilibrium theory analysis, explicit equations to calculate productivity are derived for systems following a linear isotherm. Specific conditions under which the BP-SMB provides significant advantages are elucidated. The effect of column efficiency and feed concentration for systems following non-linear isotherms are studied using numerical simulations. The production of High-fructose corn syrup, an industrial application of BP-SMB, is analysed.

*Corresponding author

Email address: arvind.rajendran@ualberta.ca (Arvind Rajendran)

Keywords: Simulated moving bed chromatography, Reduced purity, Equilibrium theory, Sugar separations, Triangle theory

1. Introduction

Chromatographic processes are often used for separations that result in products of very high purities e.g., enantiomer separations [Nicoud, 2015]. The simulated moving bed chromatography (SMB) process that was originally developed for petrochemical separations was later expanded to sugar separations and to pharmaceutical purifications [Ruthven and Ching, 1989, Rajendran et al., 2009]. The ability of the SMB to produce high-purity products, at high-productivity and reduced solvent consumption, with the use of low-efficiency columns was one of the primary reasons for its rapid acceptance in the industry. In the last 20 years, the technology has matured with proven applications in binary and ternary separations [Rajendran, 2013, Nicoud, 2014].

The study of SMB has focussed on designing the process for high-purities (excess of 99%). However, there are situations where the SMB is tasked with the production of reduced purity products, i.e., purity $< 100\%$. This happens in the case of hybrid processes where the SMB performs the bulk separation and another process, e.g., crystallization purifies the product further [Nicoud, 2015, Amanullah and Mazzotti, 2006] and in processes where lower purity products have commercial value, e.g., the production of high-fructose corn syrup (HFCS) [Nicoud, 2015]. In this separation, the outlet of an isomerization reactor containing 42% fructose and 58% glucose, is fed to a SMB. The feed is resolved into a raffinate stream that has a glucose

purity of 90% and an extract with fructose purity of 55%. The extract is the product of commercial interest, while the raffinate product is recycled to the isomerization reactor. In practice, this separation is operated in an interesting manner, where the extract product is over-purified, e.g., up to a purity of 90% fructose and is blended with the feed stream that is "by-passed" in order to produce the target 55% HFCS product [Nicoud, 2015]. This configuration, that will be referred to as "Bypass SMB" (BP-SMB), provides additional degrees of freedom to produce low purity products by over-purifying them with the feed to reach the target-purity. Siitonen et al, described a single-column version of this concept (bypass chromatography) and developed explicit design methods for systems that follow linear and Langmuir isotherms [Siitonen et al., 2012, 2013]. They also explored conditions under which bypass chromatography provides advantages over a chromatographic separation that directly provides products that meet the target purities. It was shown that the productivity of bypass chromatography was superior to the reduced purity chromatography process under the following conditions: when low purities of the two products are required; when the feed composition is further from being an equimolar mixture, when the total concentration of the feed is low and when the column efficiency is high.

The main goal of this manuscript is to extend the analysis of the bypass-chromatography to that of BP-SMB. Explicit design equations are developed within the framework of the triangle-theory, for the case of linear isotherms [Rajendran et al., 2009, Mazzotti et al., 1997]. Numerical simulations are used to validate the design method and extend it to the case of

non-linear isotherms. Case studies are performed in order to identify conditions under which the BP-SMB provides advantage over the classical SMB. The case of HFCS manufacture is discussed in detail.

2. Bypass-SMB: System description and modeling

2.1. System description

The system considered in this study is described in Fig. 1. It consists of a classical four-section SMB with the provision of using multiple columns in each section coupled with a blending section. The feed consists of a binary mixture of two species: the strongly adsorbing component "A" and the weekly adsorbing component "B" dissolved in a non-adsorbing desorbent. The concentration component i in the feed is ${c_i}^{\mathrm{F}}$. The feed is introduced between sections 2 and 3, which perform the separation duty. Sections 1 and 4 are responsible for regenerating the solid and fluid phases, respectively. The desorbent is introduced into section 1 and leaves section 4. In many practical situations, the desorbent leaving section 4 is externally regenerated to remove the impurities and recycled to section 1. In this work, we restrict ourselves to the case of an open-loop configuration, i.e., one in which the desorbent is not recycled. The raffinate product, which consists of the product enriched in B, is recovered between sections 3 and 4, while the extract product, which is enriched in A, is recovered between sections 1 and 2. The inlet and outlet ports are switched in the direction of the fluid flow to simulate the countercurrent movement of the solid and fluid phases. In the current case, the purity of the extract and raffinate streams obtained from the SMB,

denoted as $Pu_{\mathrm{E}}^{\mathrm{SMB}}$ and $Pu_{\mathrm{R}}^{\mathrm{SMB}}$, respectively are defined as:

$$Pu_{\mathrm{E}}^{\mathrm{SMB}} = \frac{n_{\mathrm{A,E}}^{\mathrm{SMB}}}{n_{\mathrm{A,E}}^{\mathrm{SMB}} + n_{\mathrm{B,E}}^{\mathrm{SMB}}} \tag{1}$$

and

$$Pu_{\mathrm{R}}^{\mathrm{SMB}} = \frac{n_{\mathrm{B,R}}^{\mathrm{SMB}}}{n_{\mathrm{A,R}}^{\mathrm{SMB}} + n_{\mathrm{B,R}}^{\mathrm{SMB}}} \tag{2}$$

In the above equations n represents the number of moles of a particular species collected within one switch (the switch time is denoted as t^*).

The SMB is considered to have identical columns each of length L, volume V and void fraction ε. Each section of the SMB has a unique internal flow rate Q_j, with $j = 1...4$ representing the different sections of the SMB. The internal and external flow rates are related by the following nodal balances:

$$Q_1 = Q_{\mathrm{D}} \tag{3}$$

$$Q_2 = Q_1 - Q_{\mathrm{E}} \tag{4}$$

$$Q_3 = Q_2 + Q_{\mathrm{F}} \tag{5}$$

$$Q_4 = Q_3 - Q_{\mathrm{R}} \tag{6}$$

The difference between a reduced purity SMB (RP-SMB), a process where the SMB produces the target products, and a BP-SMB is the flexibility to blend the feed with either one, or both, products in order to reach the target purities of the process, $Pu_{\mathrm{E}}^{\mathrm{tgt}}$ and $Pu_{\mathrm{R}}^{\mathrm{tgt}}$. In the case of RP-SMB, $Pu_{\mathrm{E}}^{\mathrm{SMB}} = Pu_{\mathrm{E}}^{\mathrm{tgt}}$ and $Pu_{\mathrm{R}}^{\mathrm{SMB}} = Pu_{\mathrm{R}}^{\mathrm{tgt}}$, while in the case of BP-SMB $Pu_{\mathrm{E}}^{\mathrm{SMB}} \geq Pu_{\mathrm{E}}^{\mathrm{tgt}}$ and $Pu_{\mathrm{R}}^{\mathrm{SMB}} \geq Pu_{\mathrm{R}}^{\mathrm{tgt}}$. The volume of feed bypassed to the extract and raffinate

products, denoted as $V_{\mathrm{E}}^{\mathrm{BP}}$ and $V_{\mathrm{R}}^{\mathrm{BP}}$, respectively can be be calculated as:

$$V_{\mathrm{E}}^{\mathrm{BP}} = \frac{Pu_{\mathrm{E}}^{\mathrm{tgt}}\left(n_{\mathrm{A,E}}^{\mathrm{SMB}} + n_{\mathrm{B,E}}^{\mathrm{SMB}}\right) - n_{\mathrm{A,E}}^{\mathrm{SMB}}}{{c_{\mathrm{A}}}^{\mathrm{F}} - Pu_{\mathrm{E}}^{\mathrm{tgt}}\left({c_{\mathrm{A}}}^{\mathrm{F}} + {c_{\mathrm{B}}}^{\mathrm{F}}\right)} \tag{7}$$

$$V_{\mathrm{R}}^{\mathrm{BP}} = \frac{Pu_{\mathrm{R}}^{\mathrm{tgt}}\left(n_{\mathrm{A,R}}^{\mathrm{SMB}} + n_{\mathrm{B,R}}^{\mathrm{SMB}}\right) - n_{\mathrm{B,R}}^{\mathrm{SMB}}}{{c_{\mathrm{B}}}^{\mathrm{F}} - Pu_{\mathrm{R}}^{\mathrm{tgt}}\left({c_{\mathrm{A}}}^{\mathrm{F}} + {c_{\mathrm{B}}}^{\mathrm{F}}\right)} \tag{8}$$

3. Modelling

From the above description, it is evident that BP-SMB is nothing but a standard SMB coupled with a blending step. In order to numerically simulate the operation of a SMB, the following assumptions are made :

1. There are no radial concentration gradients along the columns.
2. The system is isothermal.
3. Fluid velocity is constant in each column.
4. Column properties are constant and identical throughout the unit.
5. Local equilibrium is assumed between fluid and solid concentrations.
6. All mass transfer effects are modelled using the axial dispersion coefficient.

The above set of assumptions result in what is traditionally referred to as the 1D equilibrium-dispersive model. The component mass balance is provided by :

$$D_{L,i,j}\frac{\partial^2 c_i}{\partial z^2} - v_j\frac{\partial c_i}{\partial z} - \frac{\partial}{\partial t}\left[c_i + \frac{1-\varepsilon}{\varepsilon}q_i^*\right] = 0 \tag{9}$$

where v_j is the interstitial fluid velocity in section j, ε is the column void fraction, q_i^* is the solid phase loading in equilibrium with the fluid phase con-

centration C_i, and $D_{L,i,j}$ is the velocity-dependent axial dispersion coefficient. The above equation can be solved using a set of initial conditions and the well-known Danckwert's boundary conditions [Rajendran et al., 2009]. For a specific set of operating conditions, the SMB can be simulated by writing a component balance for each of the solutes and coupling the mass balances with the nodal balances. The SMB process is simulated until cyclic steady state is reached and all performance indicators are calculated under this condition. In this work, Eq. 9 was discretized in the axial direction using a finite volume technique, where each column was divided into 50 control volumes. The resulting ordinary differential equation was then solved using the inbuilt MATLAB solver *ode45*.

4. Design of reduced-purity SMBs

The design of classical SMB can be performed using the well-known "triangle-theory" [Rajendran et al., 2009, Mazzotti et al., 1997], which is based on the equilibrium theory of chromatography [Rhee et al., 2001, Mazzotti and Rajendran, 2013]. The design is based on the concept of a true-moving bed (TMB) together with the application of the SMB-TMB equivalence relationships. The triangle theory relies on the concept of the dimensionless flow rate ratios, m_j, defined for each section of the SMB:

$$m_j = \frac{Q_j t^* - V\varepsilon}{V(1-\varepsilon)} \tag{10}$$

For systems that follow a linear isotherm, i.e., when:

$$q_i^* = H_i c_i \tag{11}$$

where H_i is the Henry constant of component i, the necessary conditions to ensure complete separation, i.e. $Pu_{\mathrm{E}}^{\mathrm{SMB}} = Pu_{\mathrm{R}}^{\mathrm{SMB}} = 100\%$, while satisfying solid and fluid phase regeneration requirements, is given by the set of constraints:

$$H_A \leq m_1 \tag{12}$$

$$H_B < m_2 \leq H_A \tag{13}$$

$$H_B \leq m_3 \leq H_A \tag{14}$$

$$m_4 \leq H_B \tag{15}$$

The constraints on m_2 and m_3 can be plotted as shown in Fig. 2. In this figure, the triangular region RSU represents the space where constraints on m_2 and m_3 are fulfilled. Operating within this triangular region while simultaneously satisfying constraints on m_1 and m_4 guarantees the complete separation of the feed into pure extract and raffinate streams. From the definition of m_j, it can be immediately recognized that the difference $m_3 - m_2$ is proportional to the feed flow and hence the vertex of the triangle, i.e., point "U", represents the operating condition that maximizes the productivity.

Rajendran derived explicit design equations for linear RP-SMB [Rajendran, 2008]. The regions on the $m_2 - m_3$ plane that guarantees a purity of $Pu_{\mathrm{E}}^{\mathrm{SMB}}$ (with $Pu_{\mathrm{E}}^{\mathrm{SMB}} < 100\%$) and $Pu_{\mathrm{R}}^{\mathrm{SMB}}$ (with $Pu_{\mathrm{R}}^{\mathrm{SMB}} < 100\%$) are given by the line segments "STP" and "RQP", respectively. It is worth noting that while there is a wide operating range to obtain complete separation, there is just one unique location where target reduced purities can be achieved for both extract and raffinate, i.e., point P. This situation makes the production

of reduced purity products directly from the SMB very challenging. The space within with pentagonal region "PQRST" guarantees that the extract and raffinate products are at purities greater than $Pu_{\mathrm{E}}^{\mathrm{tgt}}$ and $Pu_{\mathrm{R}}^{\mathrm{tgt}}$. This region can be easily constructed by calculating two auxiliary Henry constants H_{A}^{*} and H_{B}^{*} defined as:

$$H_{\mathrm{A}}^{*} = \frac{H_{\mathrm{B}} {c_{\mathrm{B}}}^{\mathrm{F}} (Pu_{\mathrm{R}}^{\mathrm{tgt}} - 1) + H_{\mathrm{A}} {c_{\mathrm{A}}}^{\mathrm{F}} Pu_{\mathrm{R}}^{\mathrm{tgt}}}{{c_{\mathrm{B}}}^{\mathrm{F}} (Pu_{\mathrm{R}}^{\mathrm{tgt}} - 1) + {c_{\mathrm{A}}}^{\mathrm{F}} Pu_{\mathrm{R}}^{\mathrm{tgt}}} \tag{16}$$

$$H_{\mathrm{B}}^{*} = \frac{H_{\mathrm{B}} {c_{\mathrm{B}}}^{\mathrm{F}} Pu_{\mathrm{E}}^{\mathrm{tgt}} + H_{\mathrm{A}} {c_{\mathrm{A}}}^{\mathrm{F}} (Pu_{\mathrm{E}}^{\mathrm{tgt}} - 1)}{{c_{\mathrm{B}}}^{\mathrm{F}} Pu_{\mathrm{E}}^{\mathrm{tgt}} + {c_{\mathrm{A}}}^{\mathrm{F}} (Pu_{\mathrm{E}}^{\mathrm{tgt}} - 1)} \tag{17}$$

In this case, the maximum productivity is achieved by operating the SMB at point "P". While the determination of the region of complete separation for common non-linear isotherms such as the Langmuir isotherm can be obtained in an explicit form [Mazzotti, 2006], the calculation of boundaries for reduced purities is so far possible only through numerical simulations [Kaspereit et al., 2007, Fütterer, 2010].

Once the physical dimensions of the SMB are fixed, the design of SMB requires the calculation of the four internal flow rates, Q_j and the switch time, t^*. In order to explicitly calculate these parameters, for the case of complete separation, the four design constraints, i.e. Eqs. 12 to 15 along with a fifth constraint are used. For the case of reduced purity products Eqs. 12, 15, along with the values of m_2 and m_3 chosen within the region "PQRST" and a fifth constraint are used. The fifth constraint in both cases, is usually based either on an expression that provides flow rates that corresponds to the maximum permissible pressure drop or from the van Deemter curve that provides the condition for the flows in order to achieve the optimal column

efficiency. In this work, we use the constraint based on the maximum pressure drop, which is often referred to as a the minimum switch time design [Katsuo and Mazzotti, 2010, Jermann et al., 2012]. Here, t^* is calculated by:

$$t^* = \frac{\phi L^2}{\Delta P_{max}} \sum_{j=1}^{4} N_j (m_j(1-\varepsilon)+\varepsilon) \tag{18}$$

where ϕ is the permeability and ΔP_{max} is the maximum allowable pressure drop. Finally, once m_j and t^* are calculated, the external flow rates can be determined, using the nodal balances (Eqs. 3 to 6) and the SMB can be operated. Productivity, Pr^{SMB}, can be calculated as

$$Pr^{\mathrm{SMB}} = \frac{(m_3 - m_2)}{N_{\mathrm{tot}} t^*_{SMB}} ({c_{\mathrm{A}}}^{\mathrm{F}} + {c_{\mathrm{B}}}^{\mathrm{F}}) \tag{19}$$

and the desorbent requirement, DR^{SMB}, can be calculated as

$$DR^{\mathrm{SMB}} = \frac{1}{({c_{\mathrm{A}}}^{\mathrm{F}} + {c_{\mathrm{B}}}^{\mathrm{F}})} \left(1 + \frac{m_1 + \nu}{m_3 - m_2}\right) \tag{20}$$

5. Design of Linear BP-SMB

For the case of BP-SMB, the user may choose to operate the unit anywhere within the region PQRST, followed by a bypass stream to achieve the target purities. Note that the very fact that the unit can now be operated anywhere within the pentagon improves the robustness of the operation making it amenable to handle variations in feed quality, process disturbances, etc. Apart from the operational flexibility, the goal in this section is to explore if any advantages can be obtained in terms of productivity improvements, and if so, what are the specific conditions at which the BP=SMB can potentially

outperform the RP-SMB.

The pentagon can be divided into four regions: Region 1, given by the triangle RSU when both extract and raffinate products from the SMB are 100% pure; Region 2a, given by the triangle QRU where the extract is 100% pure and the raffinate purity is $Pu_{\mathrm{R}}^{\mathrm{tgt}} \leq Pu_{\mathrm{R}}^{\mathrm{SMB}} \leq 100\%$; Region 3a, given by the triangle STU where the raffinate is 100% pure and the extract is $Pu_{\mathrm{E}}^{\mathrm{tgt}} \leq Pu_{\mathrm{E}}^{\mathrm{SMB}} \leq 100\%$; Region 4, given by the rectangular region PQUT where $Pu_{\mathrm{R}}^{\mathrm{tgt}} \leq Pu_{\mathrm{R}}^{\mathrm{SMB}} \leq 100\%$ and $Pu_{\mathrm{E}}^{\mathrm{tgt}} \leq Pu_{\mathrm{E}}^{\mathrm{SMB}} \leq 100\%$.

For the analysis of the BP-SMB (c.f. Fig. 1), the steps used for calculating the productivity can be summarized as follows:

1. Fix m_1 and m_4 to satisfy regeneration constraints.
2. Choose an arbitrary point W ($m_{2,W}$ and $m_{3,W}$) within the Pentagonal region PQRST in Fig. 2 such that $Pu_{\mathrm{R}}^{\mathrm{SMB}} \geq Pu_{\mathrm{R}}^{\mathrm{tgt}}$ and $Pu_{\mathrm{E}}^{\mathrm{SMB}} \geq Pu_{\mathrm{E}}^{\mathrm{tgt}}$.
3. Calculate switch time, t^* based on Eq. 18.
4. Calculate feed flow rate based on $m_{2,W}$ and $m_{3,W}$ and Eq. 10.
5. Use component mass balances to calculate $n_{i,\mathrm{E}}^{\mathrm{SMB}}$ and $n_{i,\mathrm{R}}^{\mathrm{SMB}}$.
6. Calculate bypass volumes $V_{\mathrm{E}}^{\mathrm{BP}}$, $V_{\mathrm{R}}^{\mathrm{BP}}$, using Eqs. 7 and 8, respectively.
7. Calculate productivity using:

$$Pr^{\mathrm{BP-SMB}} = \frac{V(1-\varepsilon)(m_{3,W} - m_{2,W}) + V_{\mathrm{E}}^{\mathrm{BP}} + V_{\mathrm{R}}^{\mathrm{BP}}}{N_{\mathrm{tot}} V(1-\varepsilon) t^{*,BP-SMB}} (c_A^{\mathrm{F}} + c_B^{\mathrm{F}}) \quad (21)$$

8. Calculate desorbent requirement using:

$$DR^{\mathrm{BP-SMB}} = \frac{1}{(c_A^{\mathrm{F}} + c_B^{\mathrm{F}})} \left(1 + \frac{m_1 V(1-\varepsilon) + V\varepsilon}{(m_3 - m_2)V(1-\varepsilon) + V_{\mathrm{E}}^{\mathrm{BP}} + V_{\mathrm{R}}^{\mathrm{BP}}} \right) \quad (22)$$

For the case of RP-SMB, the steps required to calculate the productivity are the same as those described for BP-SMB, except that the operating point must be the one where the purities of the SMB are identical to the target purities (i.e., within triangle RSU) and since $V_{\mathrm{R}}^{\mathrm{BP}}$ and $V_{\mathrm{E}}^{\mathrm{BP}} = 0$, the productivity $Pr^{\mathrm{RP-SMB}}$ is obtained from Eq. 19.

Using the procedure mentioned above, the ratio of the productivities achieved by the BP-SMB and RP-SMB in each of the three regions can be calculated. The seemingly complex forms reduce to surprisingly simple equations:

$$\text{Region 2a}: \quad \frac{Pr^{\mathrm{BP-SMB}}}{Pr^{\mathrm{RP-SMB}}} = \frac{H_A - m_{2,W}}{H_A - H_B} \frac{t^{*,RP-SMB}}{t^{*,BP-SMB}} \tag{23}$$

$$\text{Region 3a}: \quad \frac{Pr^{\mathrm{BP-SMB}}}{Pr^{\mathrm{RP-SMB}}} = \frac{m_{3,W} - H_B}{H_A - H_B} \frac{t^{*,RP-SMB}}{t^{*,BP-SMB}} \tag{24}$$

$$\text{Region 4}: \quad \frac{Pr^{\mathrm{BP-SMB}}}{Pr^{\mathrm{RP-SMB}}} = \frac{t^{*,RP-SMB}}{t^{*,BP-SMB}} \tag{25}$$

In Eqs. 23 to 25, the ratio of switch times for the RP-SMB and BP-SMB play a critical role in determining the ratio of productivities between the two processes, hence it is important to understand how they vary. Equation 18 can be written as

$$m_3 = -\frac{N_2}{N_3} m_2 - \left[\frac{t^* \Delta P_{\max}}{\phi L^2 \varepsilon} - \sum_{j=1}^{4} N_j - \nu(N_1 m_1 + N_4 m_4) \right] \tag{26}$$

Once the column configuration, the maximum allowable pressure drop and the values of m_1 and m_4 are fixed, Eq. 26 represents a family of straight lines on the $m_2 - m_3$ plane with a slope of $-N_2/N_3$ with t^* being the varying

parameter (see Fig. 3). As one moves from the top-right corner of the m_2-m_3 plane to the bottom left, the value of t^* decreases. Now, let us consider how the productivity ratio will vary in each of the three regions identified above. Note that the point "P" represents the only possible operating condition of the RP-SMB. In Region 2a, by observing that the term $\frac{H_A-m_{2,W}}{H_A-H_B}$ approaches its maximum value of 1 along the line "QU", and the point "U" represents the point which can be operated at the shortest switch time, it is easy to deduce that best productivity is achieved by operating the BP-SMB at point U. Note that operating at U does not guarantee a productivity larger than the RP-SMB, but is the best operating point within region 2a. Similarly it can be shown that point "T" is the best operating condition for both regions 3a and 4. Comparing points T and U, we can deduce that T would offer higher productivity for a simple reason that the switch time corresponding to T will always be shorter than that corresponding to point U. A more detailed analysis of where the BP-SMB will offer higher productivities compared to the RP-SMB can be obtained based on the nature of Eqs. 23 to 25 and Eqn 26. However, from a practical perspective, it would suffice to conclude that point T is the point of interest. In other words, the highest productivity ratio, for the case of an infinitely efficient column, is obtained when the SMB is designed to provide an extract that corresponds to the target purity and the raffinate is pure followed by blending the feed with the raffinate to obtain the target purity. This observation is consistent with the results obtained for single-column bypass chromatography [Siitonen et al., 2012]. Summarizing, the maximum ratio of the BP-SMB and RP-SMB productivities, operated

at points P and R, respectively, is given by:

$$\frac{Pr^{\mathrm{BP-SMB,T}}}{Pr^{\mathrm{RP-SMB,P}}} = \frac{\nu(N_1 H_{\mathrm{A}} + N_2 H_{\mathrm{B}}^{*} + N_3 H_{\mathrm{A}}^{*} + N_4 H_{\mathrm{B}}) + \sum_{j=1}^{4} N_j}{\nu(N_1 H_{\mathrm{A}} + N_2 H_{\mathrm{B}}^{*} + N_3 H_{\mathrm{A}} + N_4 H_{\mathrm{B}}) + \sum_{j=1}^{4} N_j} \tag{27}$$

which can be rearranged to yield

$$\frac{Pr^{\mathrm{BP-SMB,T}}}{Pr^{\mathrm{RP-SMB,P}}} = 1 + \frac{\nu N_3 (H_{\mathrm{A}}^{*} - H_{\mathrm{A}})}{\nu(N_1 H_{\mathrm{A}} + N_2 H_{\mathrm{B}}^{*} + N_3 H_{\mathrm{A}} + N_4 H_{\mathrm{B}}) + \sum_{j=1}^{4} N_j} \tag{28}$$

The second term on the RHS of the above equation is always positive and hence the BP-SMB can always be designed to provide a higher (or at least equal) productivity compared to the RP-SMB.

Finally, using a similar approach, for the case where the the BP-SMB and RP-SMB are operated with identical m_1, it can be shown that the ratio of the desorbent requirements are given by:

$$\text{Region 2a}: \ \frac{DR^{\mathrm{BP-SMB}}}{DR^{\mathrm{RP-SMB}}} \geq 1 \tag{29}$$

$$\text{Region 3a}: \ \frac{DR^{\mathrm{BP-SMB}}}{DR^{\mathrm{RP-SMB}}} \geq 1 \tag{30}$$

$$\text{Region 4}: \ \frac{DR^{\mathrm{BP-SMB}}}{DR^{\mathrm{RP-SMB}}} = 1 \tag{31}$$

These are quite interesting results that show that the BP-SMB does not provide any advantage in terms of solvent consumption. This again is fully consistent with the observations made for bypass-chromatography [Siitonen et al., 2012]. Specifically, the desorbent requirement in region 4, where productivity advantages are seen does not disadvantage the BP-SMB in terms of desorbent requirement, while providing the additional possibility to improve

productivity.

5.1. Validation of the linear BP-SMB design

Prior to proceeding with the analysis of the BP-SMB, it is important to confirm that the design equations derived in the previous section are indeed correct. In order to demonstrate this we consider the separation of Tröger's base enantiomers on microcrystalline cellulose acetate [Amanullah and Mazzotti, 2006]. As an aside, there is no specific reason to choose this system, other than the fact that it has been well characterized and used in our previous studies [Siitonen et al., 2012]. The adsorption isotherms of the two enantiomers are given by

$$(+)\text{TB} : q_{\text{A}}^{*} = \frac{6.45 c_{\text{A}}}{1 + 0.39 c_{\text{A}} + 0.065 c_{\text{A}}} \tag{32}$$

$$(-)\text{TB} : q_{\text{B}}^{*} = \frac{2.18 c_{\text{B}}}{1 + 0.39 c_{\text{A}} + 0.065 c_{\text{A}}} \tag{33}$$

where c_i is the fluid phase concentration in g/L. Under linear conditions, $H_{\text{A}} = 6.45$ and $H_{\text{B}} = 2.18$.

The specific SMB configuration considered is provided in Table 1. For this situation the productivity ratios calculated for target purities of using Eqs. 23 to 25 for $Pu_{\text{R}}^{\text{tgt}} = Pu_{\text{E}}^{\text{tgt}} = 75\%$ are shown in Fig. 3 (a). The contours clearly indicate that for this case, certain portions of regions 3a (STU) and 4 (PQUT) where the BP-SMB has a higher productivity compared to RP-SMB. Further, the maximum productivity ratio corresponds, as predicted, to point T. In order to confirm the analytical solutions, numerical simulations were performed using very low values of D_{L} and a large number of finite

volumes. The $m_2 - m_3$ plane was discretized into hundreds of points (shown as dots in Fig. 3 (b)). For each of these points, the minimum switch time was calculated using Eq. 18 and the SMB was simulated numerically until cyclic steady state was reached. Based on the mass balances, the bypass volumes were calculated which yielded the value of productivity. The productivity ratios obtained from the numerical simulations (lines) and analytical equations (symbols) are superimposed in Fig. 3 (b). The comparison shows the excellent match between the two approaches, thus validating the analytical expressions. Finally, Fig. 3 (c) shows the ratio of the desorbent requirements of the BP-SMB and RP-SMB obtained from the numerical simulations. This plot confirms the expectations that, specifically in Region 4, the desorbent requirements for both the BP-SMB and RP-SMB are identical.

5.2. Analysis of Linear BP-SMB under ideal conditions

Enabled by the derivation of the maximum productivity ratio and confirmation using numerical simulations, it is now possible to analyse conditions under which the BP-SMB provides advantages over the RP-SMB. From Eq. 28, it is quite clear that the a number of factors such as the number of columns in each section, the Henry constants, the feed compositions of the two components and the expected target purities influence the choice. In the following analysis, we consider cases where the number of columns in each section of the SMB are identical and that the conditions of $m_1 = H_{\mathrm{A}}$ and $m_4 = H_{\mathrm{B}}$ are imposed. Note that these two conditions provide the lower limits for m_1 and m_4. Increasing these values will diminish the advantage of the BP-SMB as it can be clearly inferred from Eq. 28. For the following three case studies, the base case considered is the separation of a Tröger's base

racemic mixture with target purities of 75% for both raffinate and extract.

As the first case study, we explore the effect of the target purities on the advantage of a BP-SMB. Figure 4 (a) shows the contours of the productivity ratio as function of the extract and raffinate purity operated at point T. The figure clearly illustrates the fact that the BP-SMB is naturally preferred only when the target extract and raffinate purities are low. It is also interesting to see that the target raffinate purity has a higher impact on the productivity ratio as compared to the extract purity. For a given extract purity the productivity ratio is a strong function of the raffinate purity. However, for a given raffinate purity, the productivity ratio only weakly depend on the extract purity. In order to illustrate this we consider three unique scenarios that are represented by the blue, black and yellow circles in Fig. 4 (a). Since the Henry constants are identical for all of the three scenarios, the pentagons originate from the diagonal at identical values of H_{A} and H_{B} (c.f. Fig. 4 (b)). Between the blue and yellow points, note that vertices of P and T, the best operating conditions for the RP-SMB and BP-SMB, respectively are closer to each other for the yellow circle. As shown in Eq. 25 since the productivity ratio is proportional to the ratio of the switch times, we obtain lower productivity ratio corresponding to the yellow point. However, comparing the blue and black operating points for which the raffinate purities are identical, it is worth noting that the relative positions of P and T for the corresponding pentagons are nearly identical. This results in nearly identical productivity ratios.

As a second case study, the effect of the Henry constant and selectivity is considered. Figure 4 (c) shows the contours of the productivity ratio as

a function of H_A and the selectivity, $\alpha = H_A/H_B$). It is clear from the contour plot that the BP-SMB shows an advantage for systems that have high values of H_A and α. In order to illustrate the reason for the same, three different conditions are considered as shown by the circles. For each of these cases, the pentagonal region that guarantees the target purities of both purity and recovery are shown in Fig. 4 (d). When the H_A is held fixed and the selectivity is lowered (as shown by the location of the purple circle and the corresponding pentagon), the ratio of the switch times corresponding to vertices P and T of the respective pentagons are of comparable magnitudes but closer in the case of the purple pentagon. This results in a reduction of the productivity. Similarly, when the selectivity is held constant and the value of H_A is reduced (shown by the pink circle and the corresponding pentagon), the position of the pentagon moves to lower values of m_2 and m_3. First the region where the purities can be guaranteed shrinks and the location of the vertices of P and T are closer to each other. This again results in a lower productivity ratio.

As a final case study, we consider the effect of the feed composition and selectivity. First we define the solvent-free mole fraction of lighter component as $x_B = c_B/(c_A + c_B)$. Hence, when $x_B > 0.5$, the feed is rich in the lighter component and richer in the heavier component when $x_B < 0.5$. Figure 4 (e) shows the impact of x_B and the selectivity on the productivity ratio. It can be seen that the BP-SMB is advantageous for systems that are rich in the lighter component. In order to illustrate this, the region of acceptable separation for three different values of x_B are shown in Fig. 4 (f). It can be seen that for the case of $x_B = 0.5$, the pentagon is symmetric (along the axis

that is orthogonal to the diagonal and passes through the vertex). In the case of $x_{\mathrm{B}} = 0.7$, it is interesting that the the pentagon is skewed and the vertices P and T are further separated compared to the case where $x_{\mathrm{B}} = 0.4$. This clearly results in a larger productivity ratio.

Summarizing, the advantages of the BP-SMB over a RP-SMB are clearly seen under the the following conditions: when the feed is rich in the lighter component; the Henry constants of the two components are high; when the selectivity of the system is high; and when low extract and raffinate purities are desired. As shown, significant advantages can be acquired when all these conditions are met.

5.3. Effect of column efficiency

The pentagonal region delimited by the design equations seen in Fig. 2 is a very good starting point when designing a BP-SMB process. However, it is important to notice that this separation region is obtained considering columns with infinite efficiency. Real columns tend to have lower efficiency due to axial dispersion and mass transfer resistances; decreasing the purity of both light and heavy products. Hence, it is important to study the effect of column efficiency on the BP-SMB performance. Since there are no explicit analytical equations to analyse the effect of column efficiency on the performance of a SMB, a numerical approach is adopted. Conservative constraints of $m_1 = 10$ and $m_4 = 0.1$ were adopted to ensure that the regeneration requirements are conveniently met for a wide range of column efficiencies. Then the $m_2 - m_3$ plane was discretized into hundreds of points and the performance of both the BP-SMB and RP-SMB was calculated for a target purity of $Pu_{\mathrm{R}}^{\mathrm{tgt}} = Pu_{\mathrm{E}}^{\mathrm{tgt}} = 75\%$

In order to study the effect of column efficiency, an entire set of simulations were performed with the axial dispersion coefficient varying from 3.01x10^{-4} to 3.01x10^{-1} cm^2/s. For each case of the axial dispersion coefficient, a pulse injection on a single column was simulated to calculate the number of theoretical plates per column. The results of this study are shown in Fig. 5 (a), where the maximum productivity ratios and the corresponding product purities (i.e., $Pu_{\mathrm{E}}^{\mathrm{BP-SMB}}$ and $Pu_{\mathrm{R}}^{\mathrm{BP-SMB}}$) are plotted as a function of their respective number of theoretical plates. First, it can be noted that the productivity ratio decreases as the column efficiency drops. At very low values of column efficiency, the analysis shows that there is no productivity advantage to be gained from the BP-SMB. The asymptotic approach of the maximum productivity ratio curve to the value obtained for an ideal scenario (denoted by the red dashed line and calculated with Eq. 28) is another confirmation of the linear design methodology derived in the previous sections.

Figure 5 (b) shows the purity of the extract and raffinate from the SMB corresponding to the maximum productivity operating points shown in Fig. 5 (a). As the column efficiency increases, the values of the $Pu_{\mathrm{E}}^{\mathrm{BP-SMB}}$ and $Pu_{\mathrm{R}}^{\mathrm{BP-SMB}}$ at which the maximum productivity ratios are attained also approach the expected condition seen in the ideal system. The purity $Pu_{\mathrm{R}}^{\mathrm{BP-SMB}}$, initially close to 95%, drops steadily to the target raffinate purity as the column efficiency decreases. On the other hand, the values of $Pu_{\mathrm{E}}^{\mathrm{BP-SMB}}$ remain close to the extract target purity, unaffected by the axial dispersion coefficient.

In order to illustrate these observations, the cases where the number of theoretical plates are 479 and 70.5 are presented in Figs. 5 (c) and (d), respectively. By analysing the region of complete separation (represented by

the black solid lines with purities of 99%) shrinks significantly as the column efficiency drops. However, the pentagon for the reduced purity operations (represented by the solid black lines for 75% purity) from both cases are still relatively close to the ideal system (denoted by the red dashed lines). The most noticeable difference is regarding the contour of 75% raffinate purity for the low efficiency column (c.f., Fig. 5 (d)), where the curve shifts to a lower position, decreasing the operational flexibility and maximum attainable productivity ratios. The productivity ratio contours are also plotted in Fig. 5 (b) and 5 (c). From the higher efficiency system, it can be noted that there is a region enclosed between the productivity contour of 1.0 and the contour for 75% purity of extract where the BP-SMB offers improved productivity when compared to the RP-SMB (i.e., $\mathrm{Pr}^{ratio} > 1.0$). For the case where number of theoretical plates per column is 70.5, the region is nearly non-existent, implying that the operation of BP-SMB is not efficient from the perspective of productivity increase. In both scenarios, the red circles represent the m_2 and m_3 values from which the highest productivity ratios are attained. It is noticeable that in the lower efficiency case the point moves upward, backing the results seen in Fig. 5 (a) since it shows that $Pu_{\mathrm{E}}^{\mathrm{BP-SMB}}$ tends to stay constant but $Pu_{\mathrm{R}}^{\mathrm{BP-SMB}}$ decreases, therefore reducing the productivity ratio.

6. Non-linear BP-SMB

In order to analyse the effects of non-linearity in the separation system, the same Tröger's base system is considered but now with the competitive Langmuir isotherm. Two scenarios with differing column efficiencies are studied and presented in Fig. 6. In both cases, the operating region for reduced

purity shrinks and skews toward the bottom left corner on the m_2-m_3 plane. Regarding the operating regions for region of complete separation, it is noticeable in Fig. 6 (b) that the area shrinks as the efficiency drops, similar to what was seen for linear systems. However, the region where the reduced purities are obtained is affected to a lesser effect. Considering the region between the productivity ratio contour of 1.0 and the operating lines for reduced purities (i.e., solid black lines), we can conclude that there are advantages in BP-SMB from a productivity perspective in both scenarios. Even though the system with lower efficiency shown in Fig. 6 (b) presents a smaller maximum productivity ratio when compared to the higher efficiency column, it is still significantly larger than the case presented in Fig. 5 (c). The optimal operating conditions, i.e. red circles, showed again the tendency of higher productivity ratios in regions where $Pu_{\mathrm{E}}^{\mathrm{BP-SMB}} \approx Pu_{\mathrm{E}}^{\mathrm{tgt}}$ and $Pu_{\mathrm{R}}^{\mathrm{BP-SMB}} \geq Pu_{\mathrm{R}}^{\mathrm{tgt}}$.

6.1. Effect of feed concentration

To study the effects of feed concentration on the current system, parametric studies were performed by varying the feed concentration from $\mathrm{c}_i^F = 0.1$ to $\mathrm{c}_i^F = 4.5$ g/L. The maximum productivity ratios achieved in each case are plotted as a function of feed concentration in Fig. 7 (a). At low feed concentrations, the productivity ratio first increases; reaches a maximum and finally drops with further increase in concentration. To analyse this phenomenon in detail, three different case studies were chosen and their respective separation regions are plotted in Fig. 7 (b), with the optimal operating condition in each case indicated by their respective circles. The blue boundary represents a system with $\mathrm{c}_i^F = 0.3$ g/L and it is noticeable that it resembles the pentagon

obtained in linear cases, since the low concentrations reduced the effects of non-linearity in the system. The green and black curves represent a system with $c_i^F = 1.0$ and $c_i^F = 3.0$ g/L, respectively. As the feed concentration increases, the operating region shrinks and bends toward the bottom left region on the m_2-m_3 plane, going from a symmetric pentagon to the shape seen previously for non-linear systems. The initial productivity ratio increase seen in Fig. 7 (a) occurs mainly due to the fast decrease of $t^{*,BP-SMB}$ and the steady increase of $Pu_{\mathrm{R}}^{\mathrm{BP-SMB}}$ (increasing the volume bypassed toward the raffinate product) at low c_i^F. As feed concentration increases and the non-linear characteristics dominate, the shape of the operating region drastically changes causing the distance between the operating points for BP-SMB and RP-SMB to shorten at a faster rate, decreasing the productivity ratio. It is worth mentioning that for all case studies analysed the productivity ratio was higher than 1.0, showing the advantages of BP-SMB over RP-SMB from a productivity perspective.

7. Production of high-fructose corn syrup

One of the practical applications of the BP-SMB is in the production of high fructose corn syrup (HFCS), a sweetener [Nicoud, 2015]. In terms of quantity of the product produced globally, this is one of the largest applications of the SMB technology. The production of HFCS involves the isomerization reaction of glucose that produces a stream that contains 42% fructose and 58% glucose. This stream, called HFCS 42, is fed to a SMB unit that is tasked to separate the glucose (light raffinate product) and the fructose (heavy extract product). The product fructose that is sold in the

market consists of 55% fructose and the rest being glucose. This product is called HFCS 55. The raffinate, typically consisting of 90% glucose, is recycled to the isomerization reactor, while the extract is removed as the product. There are two approaches to produce HFCS 55. The first approach, referred to as Process α [Nicoud, 2015], is to operate the SMB in such a way that the extract product is HFCS 55, i.e. as a RP-SMB. The second approach, referred to as Process β, is to operate the SMB so that the extract product contains 90% fructose and blend it with HFCS 42 in order to achieve a final product that meets the requirement of HFCS 55, i.e. as a BP-SMB. In fact, it is Process β that is used in the industry. Nicoud, using a series of heuristic arguments, showed that the productivity of both these approaches are almost the same and the reasons why Process β is chosen is based only on operational issues [Nicoud, 2015]. The two main reasons he cites are the following: 1. Owing to the variation in the feed quality, the incoming feed to the SMB is not strictly 42%. By overpurifying the extract, the operator retains the flexibility to allow for some variation in the product quality that can be tackled easily not by changing the operating conditions of the SMB but by changing amount that is blended. 2. Owing to the low retention factors of both fructose and glucose, Process α would result in a situation where the flow rate in section 2 is very small (nearly zero), while that in section 1 is quite high. This drastic change in the flow rate during a switch can cause physical damage to the stationary phase, which is avoided in Process β. In this section, we analyze this separation to verify the empirical arguments.

7.1. Linear - equilibrium theory analysis

Under low concentrations, the equilibrium of fructose and glucose can be described by linear isotherms with the Henry constants being $H_{\text{fr}} = 0.46$ and $H_{\text{gl}} = 0.27$, respectively, resulting in a selectivity of $\alpha = 1.7$ [Nicoud, 2015]. Noticing from the previous discussions, it is rather obvious that the Henry constants of this system are low, the selectivity is modest and the feed is marginally enriched in the light component. Hence, the advantages of a BP-SMB separation over the RP-SMB can be expected to be rather modest. The operating points for the Processes α and β, for the case of a unit with infinite efficiency are shown in Fig. 8 as P_α and P_β, respectively. A few observations can be immediately made. The region within the pentagon where the BP-SMB proves to be better than the RP-SMB for producing a raffinate containing 90% glucose and an extract containing 55% fructose is very small. The maximum productivity ratio, which can be achieved by operating the SMB at point T and bypassing some feed, even under ideal conditions, is only 1.006. This indicates that operating a BP-SMB at its optimal condition does not offer any advantage even under ideal conditions. The productivity ratio corresponding to the point P_β is ≈ 0.95 indicating that the drop in productivity is about 5% compared to P_α. Under ideal conditions, it appears that Process α is advantageous compared to Process β using the minimum switch time design.

7.2. Modelling and simulation for non-ideal and non-linear systems

To extend the analysis of the HFCS-55 production, we now model and simulate the unit considering the equilibrium-dispersive model of chromatography. The parameters used are presented in Table 1. To avoid any loss of

fructose or glucose in the system, the m_i ratios in regions 1 and 4 are set to $m_1 = 1$ and $m_4 = 0.1$.

For a linear system, the isotherm parameters used are the same as the ones mentioned in the previous section. On the other hand, the isotherm for non-linear systems are described by Eq. 34 and 35 [Nicoud, 2015]. The following quadratic equations are fairly non-linear at high concentrations and are expressed in g/L.

$$q_{gl}{}^{*} = 0.27c_{gl} + 0.00012{c_{gl}}^{2} + 0.0001c_{gl}c_{fr} \tag{34}$$

$$q_{fr}{}^{*} = 0.46c_{fr} + 0.00012{c_{fr}}^{2} + 0.00024c_{fr}c_{gl} \tag{35}$$

The operating regions, productivity ratio contours and operating points P_α and P_β are plotted in Figs. 9 (a) and (b). In both linear and non-linear cases, the productivity advantages of BP-SMB are non-existent, as seen by the absence of a productivity ratio contour of 1.0 or higher inside the operating region (e.g., the commonly used route indicated by P_β results in a productivity ratio close to 96%). Different from what was observed earlier, operating the SMB unit at the optimal point T indicated by the design methodology (i.e. overpurified raffinate product and extract at target purity) also results in productivity ratio < 1.0.

For the separation of HFCS55, even though the feed is richer in glucose (i.e., light product), the added effects of low Henry constants, modest selectivity and high extract purity requirement (when compared to the raffinate product requirement) results in an overall low Productivity ratio, therefore, a system where there are no productivity advantages when using BP-SMB.

This analysis confirms Nicoud's observations that the main advantage of using a BP-SMB for HFCS production is purely based on operational advantages rather than any economic benefits.

8. Conclusions

A methodology to design and evaluate RP-SMB and BP-SMB based on the equilibrium theory analysis was presented. The first key observation is the fact that there is one unique operating condition where the SMB can be designed to produce purities that are lower than 100%. This inherently makes the SMB non-robust for reduced purity requirements. Since the BP-SMB allows for overpurification of the products from the SMB while retaining the option of bypassing the feed, significantly improves the robustness of the process. The second observation, which resulted from a thorough analysis is that it is possible to design the BP-SMB to be more productive, without increasing the desorbent requirement, compared to the RP-SMB. The results showed that high productivities in BP-SMB are attainable when the feed is richer in the light component, the Henry constants and selectivity are high and when low extract and raffinate purities are desired. Numerical simulations for both linear and non-linear systems validated the methodology and showed the effects of lowering column efficiency on the operating region and process performance. Low column efficiencies tend to decrease the maximum productivity and productivity ratio attainable. The optimal operating conditions are generally obtained when the extract product is close to the target purity and the raffinate product is overpurified. The results obtained for the HFCS 55 purification from both the equilibrium theory analysis and

numerical simulations supported the conclusions reached by Nicoud [Nicoud, 2015] in which BP-SMB do not provide productivity advantages over RP-SMB when purifying fructose; the main advantages are due to the improved robustness offered by the BP-SMB.

9. Notation

c	fluid phase concentration of solute [g L^{-1}]
D_L	axial dispersion coefficient [cm^2 s^{-1}]
H	Henry constant
K	equilibrium constant in Langmuir isotherm [L g^{-1}]
L	length of column [cm]
m	dimensionless flow rate ratio
n	number of moles
N	number of columns
N_{tot}	total number of columns
Pu	target product purity [%]
Pr	productivity [g g^{-1} s^{-1}]
Pr^{ratio}	productivity ratio between BP-SMB and RP-SMB
ΔP_{max}	maximum allowed pressure drop [bar]
Q	volumetric flow rate [cm^3 s^{-1}]
q^*	solid phase equilibrium concentration of solute [g L^{-1}]
t	time [s]
t^*	switch time [s]
v	interstitial velocity [cm s^{-1}]
V	volume of column [cm^3]

V^{BP}	bypassed volume [cm^3]
x	molar fraction
z	axial coordinate [cm]

Subscripts and Superscripts

D	desorbent
E	extract
F	feed
i	component
j	SMB section
R	raffinate
tgt	product target

Greek symbols

α	selectivity
ε	column void fraction
ν	phase ratio, (1-ε)/ε
ϕ	permeability [bar s cm^{-2}]

Amanullah, M., Mazzotti, M., 2006. Optimization of a hybrid chromatography-crystallization process for the separation of troger's base enantiomers. J. Chromatogr. A 1107 (1-2), 36–45.

Fütterer, M., 2010. Design of simulated moving bed plants for reduced purities. Chem. Engg. Technol. 33 (1), 21–34.

Jermann, S., Katsuo, S., Mazzotti, M., 2012. Intermittent simulated moving bed processes for chromatographic three-fraction separation. Org. Process Res. Dev. 16 (2), 311–322.

Kaspereit, M., Seidel-Morgenstern, A., Kienle, A., 2007. Design of simulated moving bed processes under reduced purity requirements. J. Chromatogr. A 1162, 2–13.

Katsuo, S., Mazzotti, M., 2010. Intermittent simulated moving bed chromatography: 1. design criteria and cyclic steady-state. J. Chromatogr. A 1217 (8), 1354–1361.

Mazzotti, M., 2006. Equilibrium theory based design of simulated moving bed processes for a generalized langmuir isotherm. J. Chromatogr. A 1126 (1-2), 311–322.

Mazzotti, M., Rajendran, A., 2013. Equilibrium theory-based analysis of nonlinear waves in separation processes. Annu. Rev. Chem. Biomol. Eng. 4, 119–141.

Mazzotti, M., Storti, G., Morbidelli, M., 1997. Optimal operation of simulated moving bed units for nonlinear chromatographic separations. J. Chromatogr. A 769 (1), 3–24.

600 Nicoud, R.-M., 2014. The amazing ability of continuous chromatography to
601 adapt to a moving environment. Ind. Eng. Chem. Res. 53 (10), 3755–3765.

602 Nicoud, R.-M., 2015. Chromatographic Processes. Cambridge University
603 Press.

604 Rajendran, A., 2008. Equilibrium theory-based design of simulated mov-
605 ing bed processes under reduced purity requirements. linear isotherms. J.
606 Chromatogr. A 1185 (2), 216–222.

607 Rajendran, A., 2013. Recent developments in preparative chromatographic
608 processes. Curr. Opin. Chem. Engg. 2, 263–270.

609 Rajendran, A., Paredes, G., Mazzotti, M., 2009. Simulated moving bed chro-
610 matography for the separation of enantiomers. J. Chromatogr. A 1216 (4),
611 709–738.

612 Rhee, H. K., Aris, R., Amundson, N. R., 2001. First-order partial differential
613 equations. Vol. I. Dover Publications, Mineola, N.Y.

614 Ruthven, D. M., Ching, C. B., 1989. Countercurrent and simulated coun-
615 tercurrent adsorption separation processes. Chem. Eng. Sci. 44 (5), 1011–
616 1038.

617 Siitonen, J., Sainio, T., Rajendran, A., 2012. Bypass chromatography–design
618 and analysis of an improved strategy for operating batch chromatography
619 processes. J. Chromatogr. A 1230, 77–92.

620 Siitonen, J., Sainio, T., Rajendran, A., 2013. Design of batch chromatography

621 for separation of binary mixtures under reduced purity requirements. J.
622 Chromatogr. A 1286, 55–68.

10. List of Table and Figure Captions

List of Tables

List of Figures

4 Case studies exploring the effect of different parameters on the productivity ratios. The column of figures on the left represents the contour plots of the productivity ratio as a function of two variables listed on the axes. The column on the right shows the separation regions for the operating conditions represented on the contour plot to their left hand side.

5 Effect of column efficiency on the performance of linear BP-SMB for the separation of a racemic mixture of Tröger's base mixture for 75% pure extract and raffinate under linear equilibrium. (a) Maximum productivity ratio and (b) purity of extract and raffinate at optimal operating conditions as a function of column efficiency. Separation region for the cases of (c) number of theoretical plates per column = 479 and (c) number of theoretical plates per column = 70.5

6 Operating regions for non-linear Tröger's base separation for 75% pure extract and raffinate under non-linear conditions with (a) number of theoretical plates per column = 479 and (b) number of theoretical plates per column= 70.5. The feed is a racemic mixture with the concentration of each solute being 3 g/L.

7 Effect of feed concentration on the performance of non-linear BP-SMB for the separation of a racemic feed of Tröger's base enantiomers. (a) Maximum productivity ratio as a function of total feed concentration. (b) Operating regions for 75%/75% target purities.

668 8 Separation region for HFCS-42 under ideal conditions showing
669 the operating points of a RP-SMB (P_α) and the BP-SMB (P_β)
670 as operated in the industry. The lower figure shows the zoom
671 of the region of interest.
672 9 HFCS-42 operating region with different target purities (90%/55%,
673 90%/90% and 99%/99% for raffinate and extract target puri-
674 ties, respectively). (a) Linear isotherm system. (b) Non-linear
675 isotherm system.

Parameter	Tröger's base system	HFCS system
Column length, L [cm]	10	10
Column diameter, d [cm]	1	1
Column void fraction, ε	0.59	0.59
Column configuration	1-1-1-1	1-1-1-1
Component feed concentration, c_i^{F} [g/L]	3 (A and B)	465 (glucose) 335 (fructose)
Axial dispersion coefficient, $D_{L,i,j}/v$	3.01 x 10^{-2}	1.00 x 10^{-2}
Maximum allowed pressure drop, $\Delta \mathrm{P}_{max}$ [bar]	40	40
Permeability, ϕ [bar.s/cm^2]	0.1	0.1

Table 1: Modelling parameters for the case studies considered.

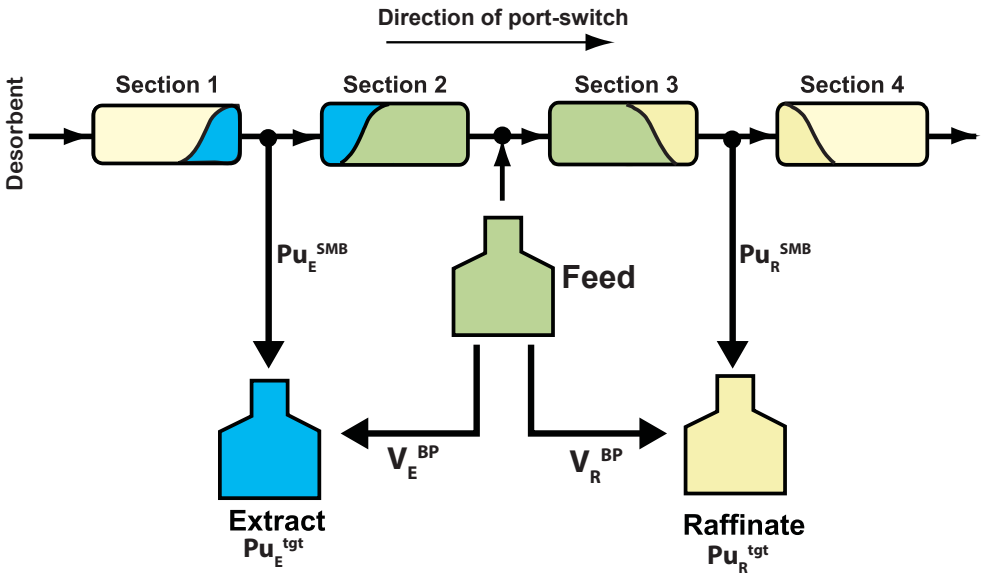

Figure 1: Schematic of the Bypass-SMB concept

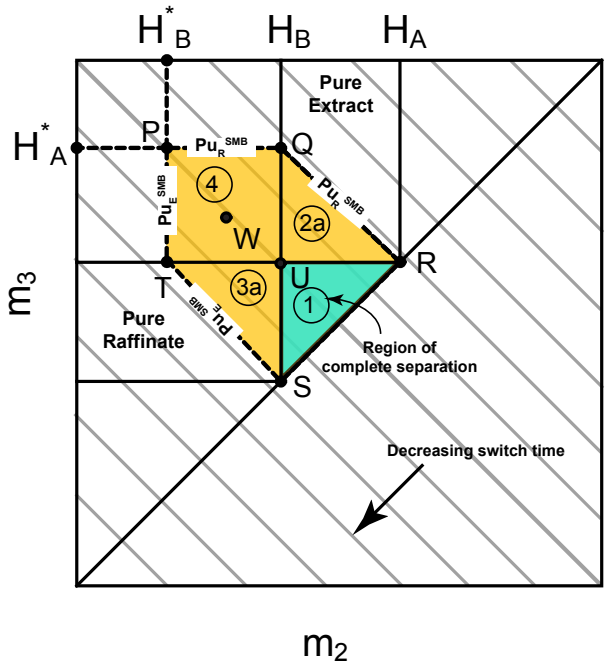

Figure 2: Separation regions for a SMB operated under reduced purities using the equilibrium theory of chromatography. The family of parallel lines for constant t^* is obtained from Eq. 26

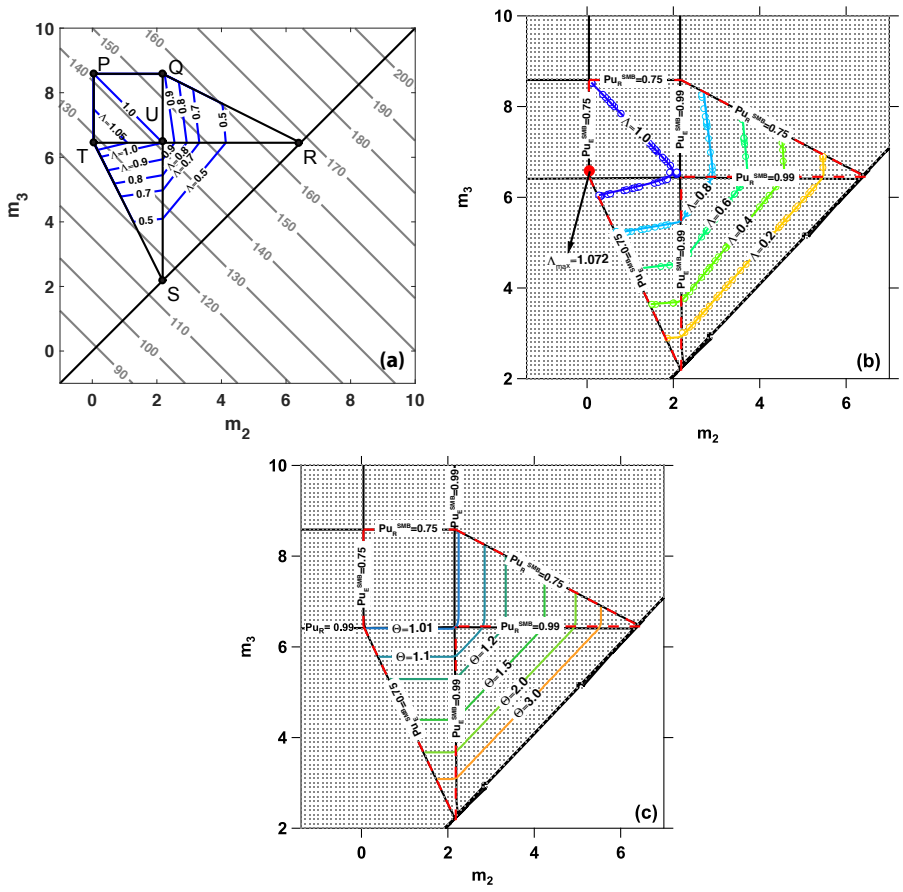

Figure 3: Validation of design equations for Linear BP-SMB (a) Contours of productivity ratio for the case of Tröger's base enantiomers under ideal conditions calculated from analytical expressions. The parallel lines for constant t^* are plotted for a $\Delta P_{max} = 40$ bar. The contours are calculated for target extract and raffinate purities of 75%; (b) Comparison between the contours of productivity ratio obtained from analytical solutions (separation region represented by red dotted lines and productivity ratio by ∘) and from numerical simulations (represented by solid lines); (c) Contours of the ratio of desorbent requirement for BP-SMB and RP-SB calculated from numerical simulations.

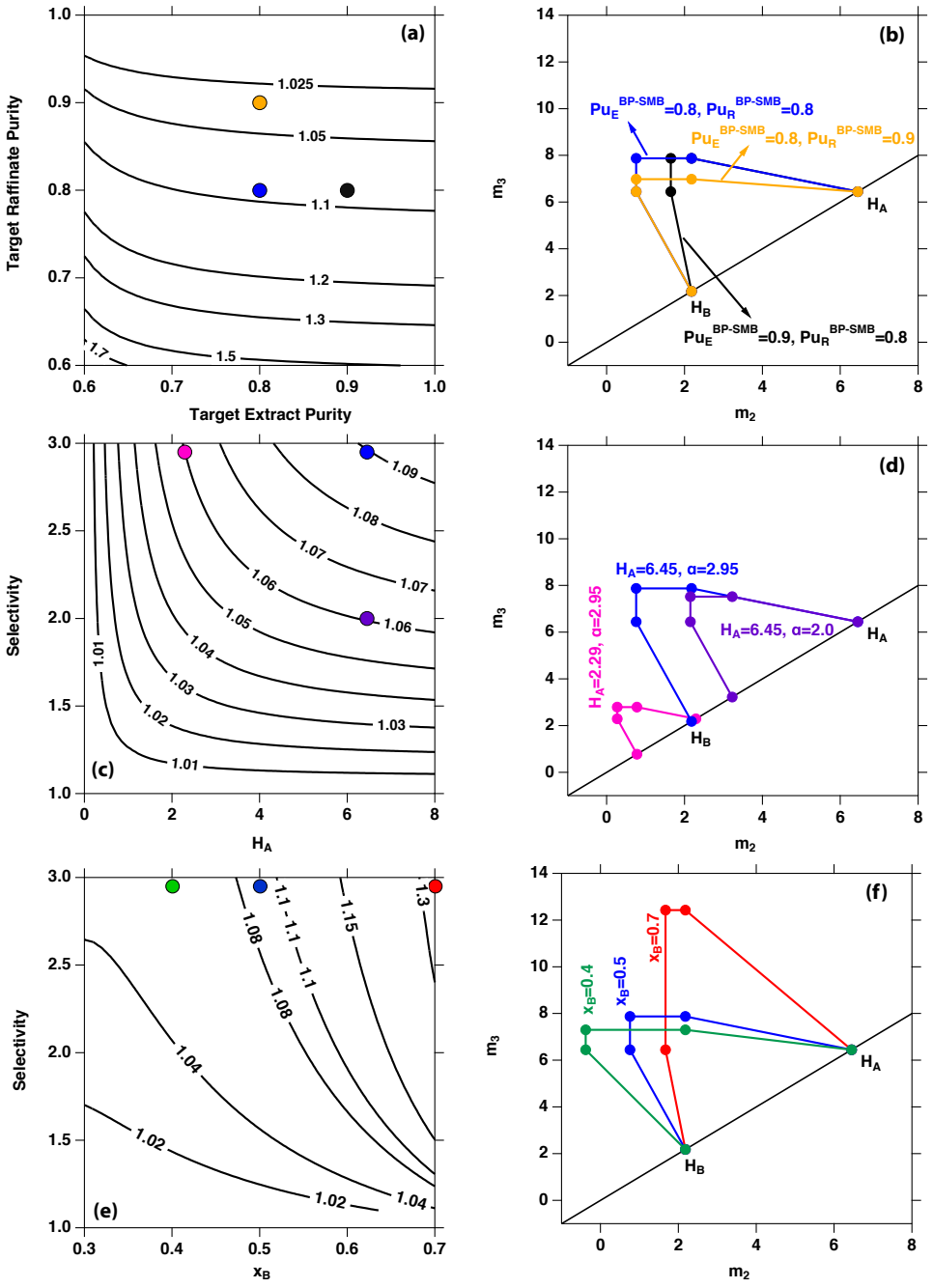

Figure 4: Case studies exploring the effect of different parameters on the productivity ratios. The column of figures on the left represents the contour plots of the productivity ratio as a function of two variables listed on the axes. The column on the right shows the separation regions for the operating conditions represented on the contour plot to their left hand side.

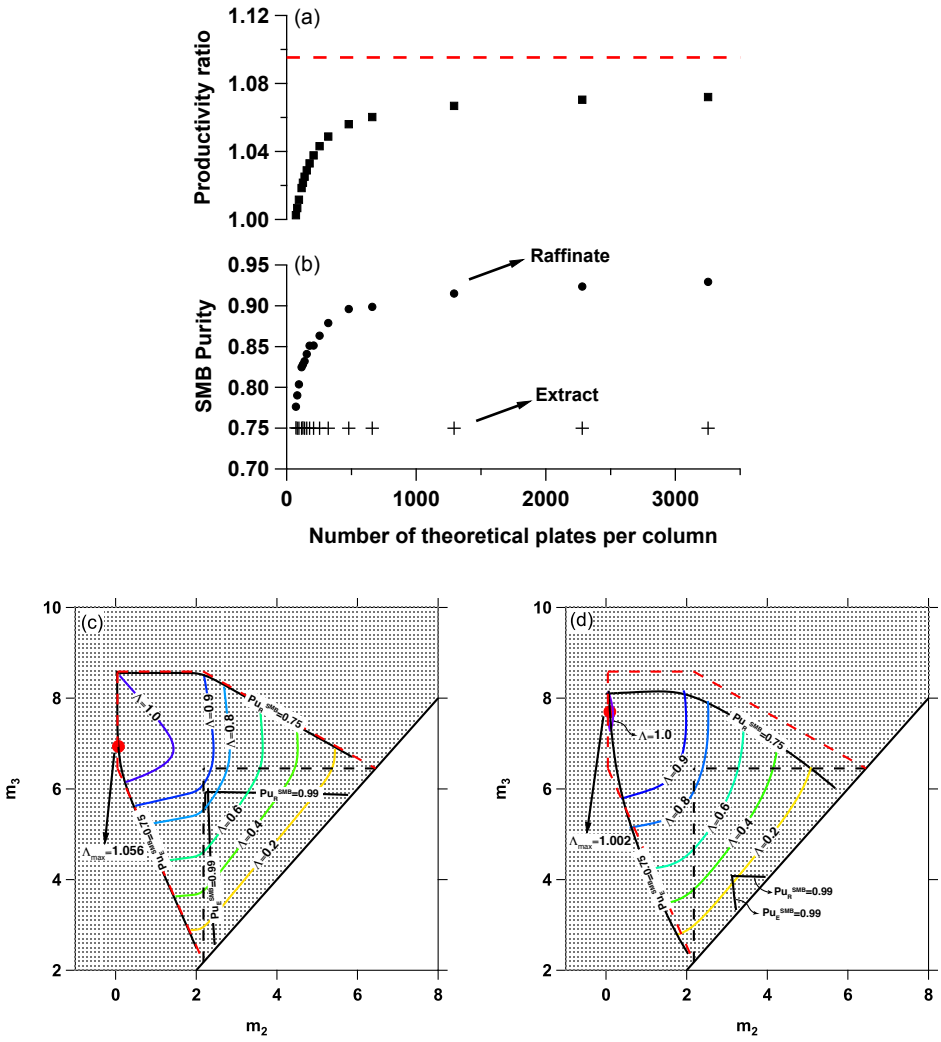

Figure 5: Effect of column efficiency on the performance of linear BP-SMB for the separation of a racemic mixture of Tröger's base mixture for 75% pure extract and raffinate under linear equilibrium. (a) Maximum productivity ratio and (b) purity of extract and raffinate at optimal operating conditions as a function of column efficiency. Separation region for the cases of (c) number of theoretical plates per column = 479 and (c) number of theoretical plates per column = 70.5

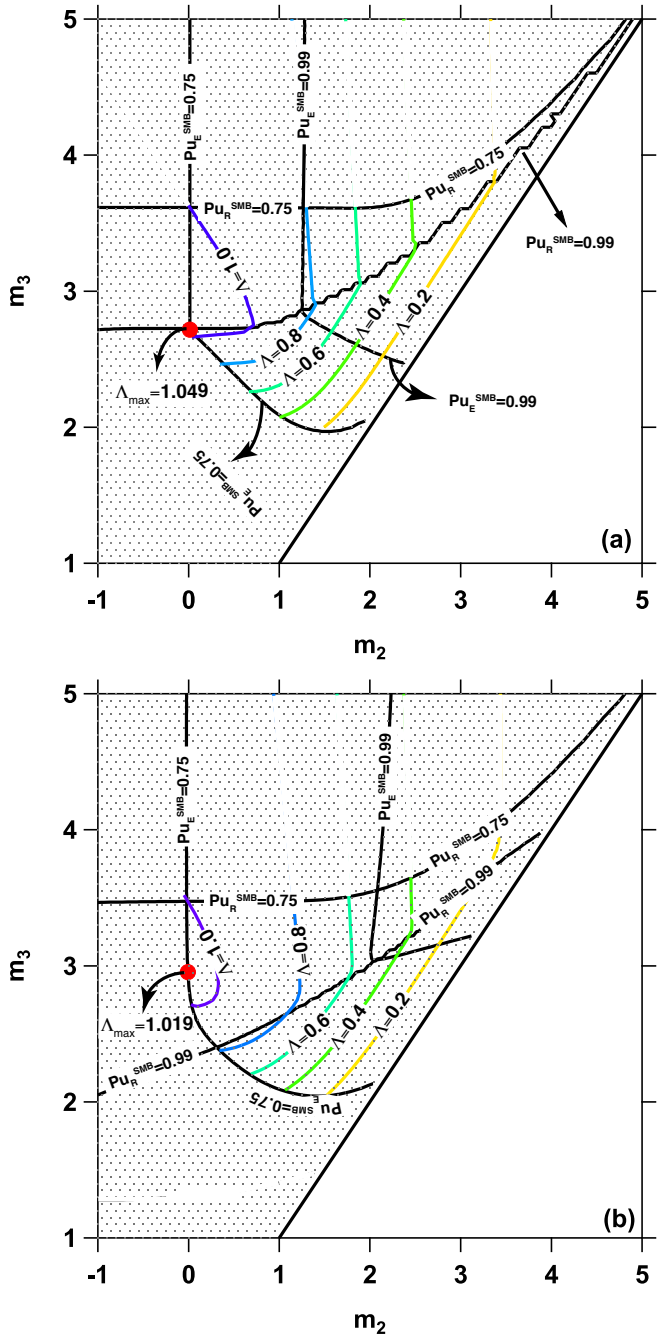

Figure 6: Operating regions for non-linear Tröger's base separation for 75% pure extract and raffinate under non-linear conditions with (a) number of theoretical plates per column = 479 and (b) number of theoretical plates per column= 70.5. The feed is a racemic mixture with the concentration of each solute being 3 g/L.

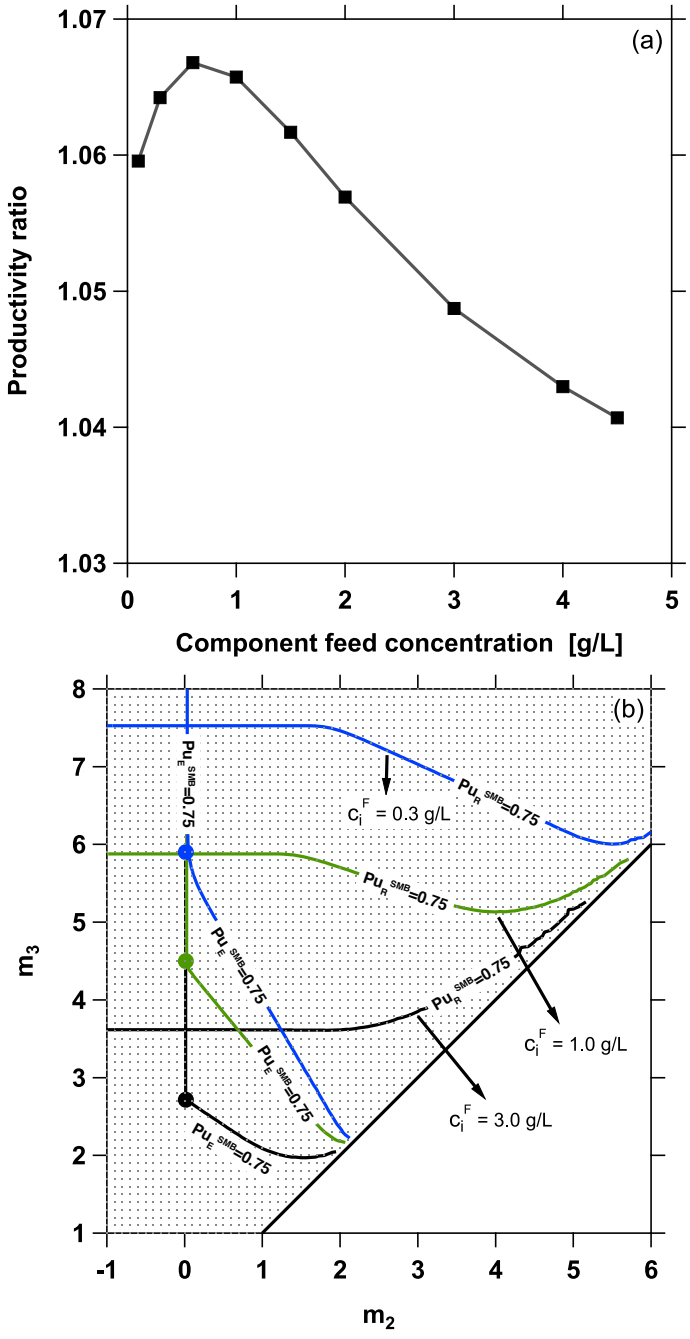

Figure 7: Effect of feed concentration on the performance of non-linear BP-SMB for the separation of a racemic feed of Tröger's base enantiomers. (a) Maximum productivity ratio as a function of total feed concentration. (b) Operating regions for 75%/75% target purities.

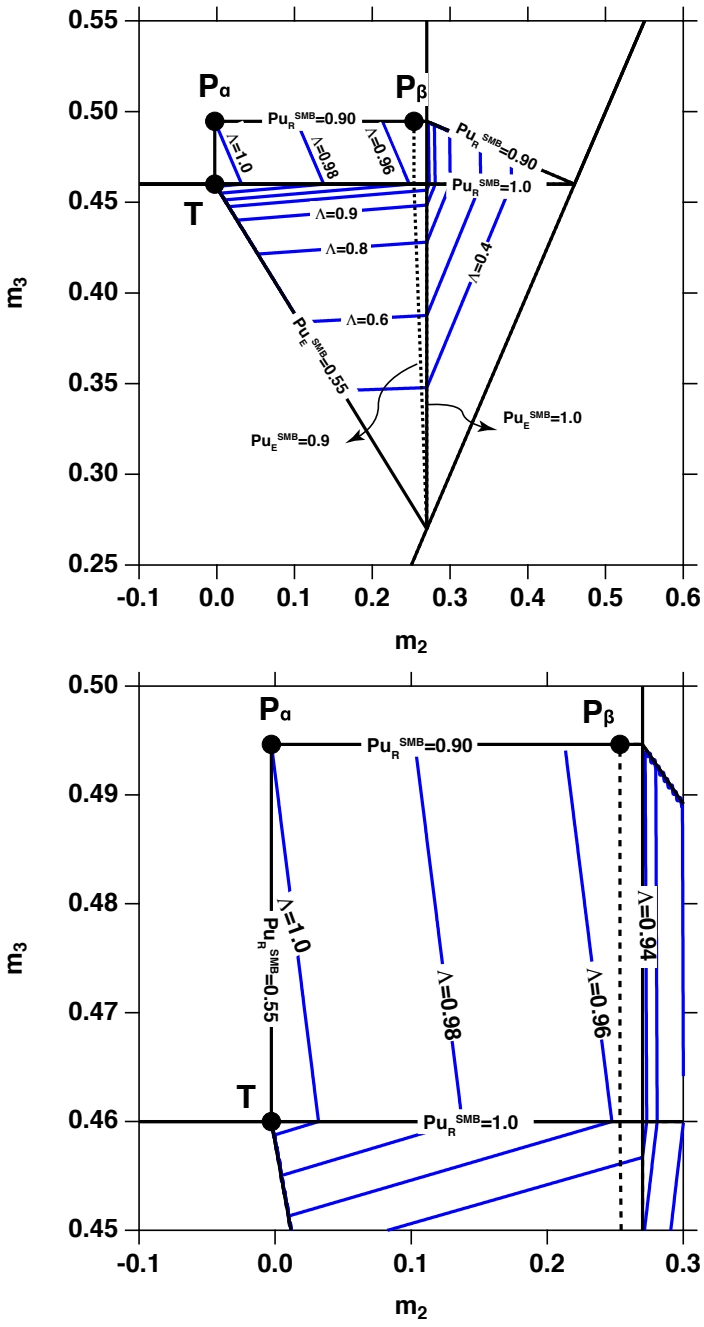

Figure 8: Separation region for HFCS-42 under ideal conditions showing the operating points of a RP-SMB (P_α) and the BP-SMB (P_β) as operated in the industry. The lower figure shows the zoom of the region of interest.

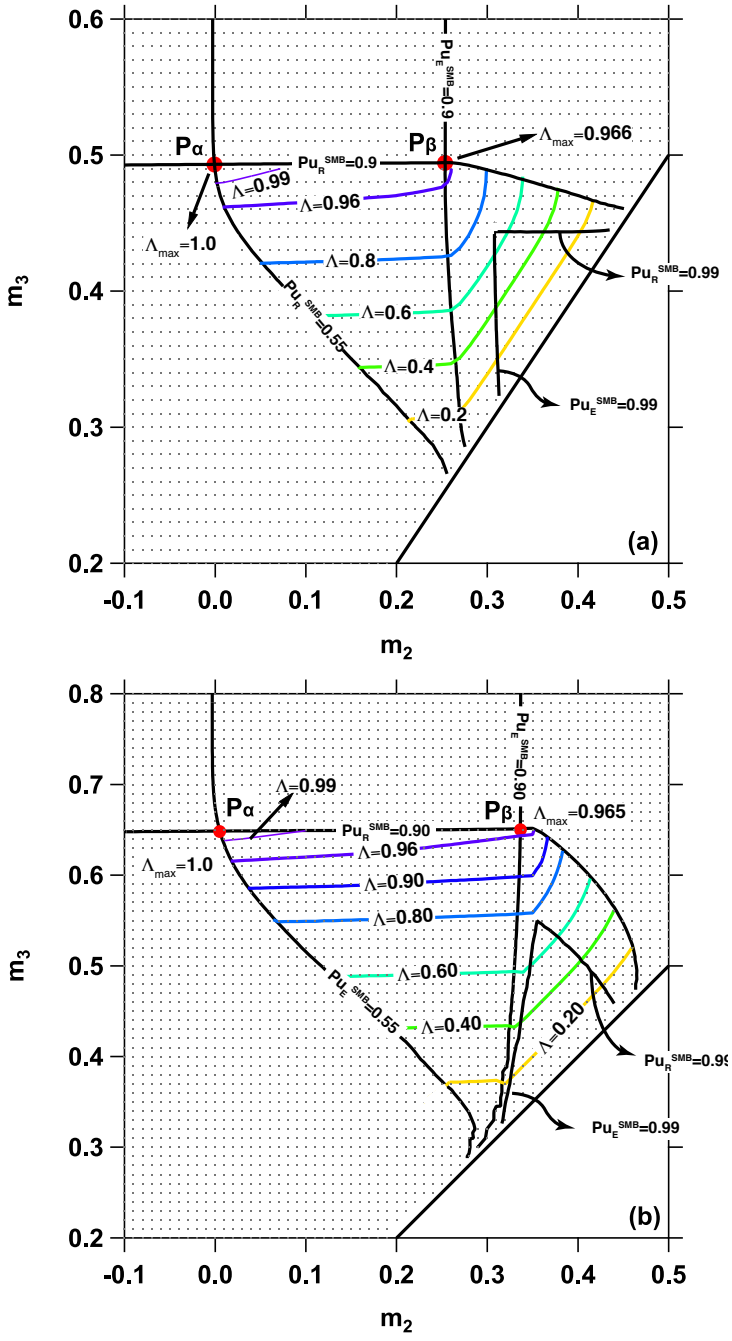

Figure 9: HFCS-42 operating region with different target purities (90%/55%, 90%/90% and 99%/99% for raffinate and extract target purities, respectively). (a) Linear isotherm system. (b) Non-linear isotherm system.